Photonics and Nanostructures - Fundamentals and Applications 50 (2022) 101023

Contents lists available at ScienceDirect

Photonics and Nanostructures - Fundamentals and Applications

journal homepage: www.elsevier.com/locate/photonics

Dimers of gold-silver core-shell nanospheres: The effect of interparticle gap on the refractive index sensitivity and extinction spectrum

Géza Szántó [a,*], Attila Bonyár [b,c], István Csarnovics [a]

[a] Department of Experimental Physics, Institute of Physics, Faculty of Science and Technology, University of Debrecen, Debrecen, Hungary
[b] Department of Electronics Technology, Faculty of Electrical Engineering and Informatics, Budapest University of Technology and Economics, Budapest, Hungary
[c] Wigner Research Centre for Physics, Budapest, Hungary

ARTICLE INFO

Keywords:
Plasmonics
Nanoparticle dimer
Core-shell bimetallic nanoparticle
Refractive index sensitivity
Localized surface plasmon resonance
Boundary element method

ABSTRACT

Gold-silver and silver-gold core-shell nanoparticle dimers were studied based on their extinction cross-section spectrum and bulk refractive index sensitivity. The simulations were performed by using the boundary element method (BEM) and the polarization direction of the used plane-wave excitation was parallel with the symmetry axis. The running parameters were the particles' outer and inner radii and their (interparticle gap/full diameter). For different particle sizes and distances, the shape of the spectra and the refractive index sensitivities are presented. In the extinction spectra, the observable peaks originate from either the gold or silver components and the most intense peak position can be distinctly assigned to one of them. A sharp boundary separates these two regions in the plane of the core radius and shell thickness parameters. It was found that by decreasing the interparticle gap, the boundary line between these two regions shifts towards the thinner shells for Ag@Au dimers, while it shifts towards the smaller cores for Au@Ag dimers. Since the sensitivity of peaks corresponding to the Au and Ag components are significantly different, the presented data can help optimize interparticle gaps concerning the core/shell thicknesses to maximize the sensitivity of nanoparticle dimers.

1. Introduction

Due to their wide applicability, there is a growing demand for developing nanomaterials in which the phenomenon of localized surface plasmon resonance (LSPR) can be created. LSPR is the collective oscillation of conduction electrons in metallic nanoparticles when excited by light at the resonant frequency. One of the most important applications of LSPR is to create sensors that detect changes in the refractive index of the medium around the particles [1,2]. The most common way to quantify the performance of such sensors is to measure or simulate the bulk refractive index sensitivity (RIS) of the nanosystem [3–6]. The bulk RI sensitivity of a wide variety of nanosystems can be found in the literature [7].

Hybrid nanostructures made from a combination of conventional metals (e.g., Au, Ag) are good candidates for improving the properties of simple metallic nanoparticles. These nanostructures are also core-shell particles created from a combination of gold and silver components that are often used in SERS applications [8–12], as well as for solar cells [13]. However, due to their simple fabrication, well-tuned resonance peak, and in many cases better sensitivity, they may also be advantageous for use as RIS sensors.

Previously the relationships between the core and shell size of monomer core-shell structures and their optical properties and sensitivity were already investigated [14]. The distance between the nanostructures is an important parameter that severely affects their sensing performance [15]. The phenomena that occur in single-metal dimer particles have already been described: the exponential shift of the peak position towards longer wavelengths with decreasing interparticle gap (plasmon ruler) [16–19], with a simultaneous increase in sensitivity [20,21].

In the case of core-shell dimers, the characteristic behavior of both core-shell particles and simple dimers is expected to appear in some modified form. Based on the plasmon hybridization theory, the basic properties of core-shell dimers can be deduced, e.g., splitting of energy levels are expected due to the core-shell structure of an individual particle [22] and also due to the presence of the second particle [23]. However, the exact optical properties of all particle systems cannot be obtained from hybridization theory because it is based on a quasi-electrostatic approximation of Maxwell's equations [24]. A more accurate description of the phenomena also requires a simulation based

* Corresponding author.
E-mail address: szanto.geza@science.unideb.hu (G. Szántó).

https://doi.org/10.1016/j.photonics.2022.101023
Received 3 May 2021; Received in revised form 23 March 2022; Accepted 29 March 2022
Available online 1 April 2022

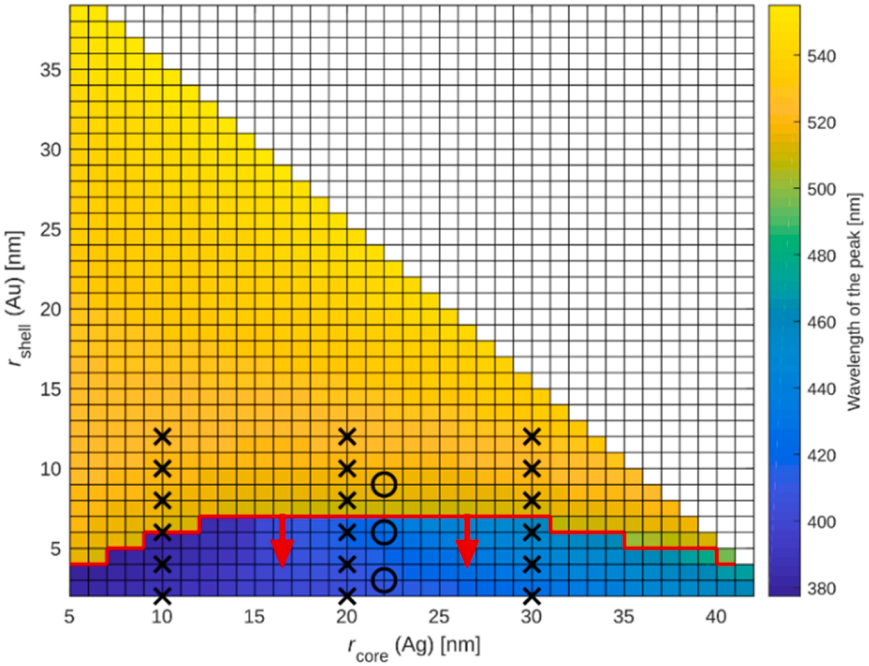

Fig. 1. The position of the most intense extinction peak as a function of core and shell radii for Ag@Au monomers. The 'O' marks indicate positions, where the effect of decreasing interparticle gap is investigated with high d/D_0 resolution (as presented in Fig. 5), 'X': indicate positions where the effect of shell thickness is investigated with lower d/D_0 resolution (as presented in Fig. 6). (Reproduced from Ref. [3] under CC-BY license).

on a time-dependent (complete) solution of Maxwell's equations.

This work aims to study the effect of the interparticle distance on the extinction spectrum and sensitivity of Au/Ag core-shell dimer nanostructures. The simplest case was selected, which means pairs made of particles with the same geometry and composition. Only Ag@Au dimers have been studied previously with a different methodology [25] and on another size and distance range. The current paper also includes the description of Au@Ag, which was not previously investigated.

2. Methods

The simulations were performed by using the boundary element method (BEM) [26]. An implementation of BEM named MNPBEM toolbox, written in MATLAB was used, which is well suited for plasmonic simulations [27]. Of the options available within the toolbox, the 'ret' solver was selected. This solver is based on the full solution of Maxwell's equations and provides accurate results.

The sensitivity and extinction cross-section spectra were studied with plane-wave excitation when the polarization direction is parallel to the symmetry axis of the two-particle system to incite the coupled plasmon modes. It has been experimentally demonstrated that better sensitivity can be achieved using the polarization scheme described in [28]. The empirical complex refractive index tables required to perform the simulations for both gold and silver were extracted from the experimental results of Johnson and Christy [29].

No corrections for size-limiting effects were taken into account in the performed simulations. The corrections may become significant for thin shells, and cores with small radii, e.g., the electron mean free path (MFP) correction [30–32]. However, in the appendix, the effect of MFP correction was evaluated by using the MATLAB code called STRATIFY [33]. The effect of the correction was found to be negligible on the results. Please see the Appendix A for a detailed comparison of MFP corrected and uncorrected results for selected cases.

As a result of the simulations, the extinction cross-section spectrum of the given particle system was obtained (between 350 nm and 1000 nm, with 1 nm wavelength resolution). The spectra were recorded for two different media to calculate the bulk refractive index sensitivity. Refractive indices $n_1 = 1.33$ and $n_2 = 1.35$ were used for the simulations. The modeled sensor operates in an aqueous medium, so n_1 is the refractive index of water. $\Delta n = (n_2 - n_1)$ was chosen small enough to allow an unambiguous pairing of the peaks observed in different media (which could have been a problem for multi-peak spectra), but large enough that the error in determining the peak positions would not significantly affect the sensitivity. The sensitivity was calculated from the shift of a peak, divided by the difference of the refractive indices ($\Delta n = 0.02$ RIU). The study of other optical properties, such as the classification of the peaks, was performed based on the spectrum in an aqueous medium (n_1). The simulation and analysis were performed in the same manner as previously described, except that particle pairs and not individual particles have been studied [14].

Instead of studying the distance dependence measured in *nm*, the data were presented as a function of the dimensionless distance/(total particle diameter): $d/D_0 = d/(2(r_c + r_s))$, where D_0 - total particle diameter, d - distance, r_c - radius of core, r_s - thickness of the shell. Sensitivity and extinction cross-section were studied as a function of three independent variables: r_c, r_s, and d/D_0. This convention is often used because of the universal scaling described in the non-core-shell case. The particles studied are large enough to perform a purely electrodynamics-based simulation on them, however, distances that are too short (typically below nm) also raise the need for quantum mechanical-based methods [34]. This problem can occur only to a small extent and only for the shortest interparticle gaps ($d/D_0 = 1/40$), around approximately 1 *nm*.

Our previous work investigated the optical properties of monomer core-shell nanoparticles and their achievable sensitivities [14]. For both material compositions, it can be observed that, depending on the r_c, r_s sizes, the gold-type peaks dominate the extinction spectra in some size ranges and the silver-type peaks in others. Silver-type (short-wavelength) peaks are from now on referred to as Ag peaks, while Au-type (long-wavelength) peaks are referred to as Au peaks. Peak types that could not be classified into the previous two categories were also found. Peaks resulting from the interaction of plasmonic modes are referred to as hybrid peaks. In the case of thicker silver shells, smaller, quadrupole attributed extinction peaks were also observed in the

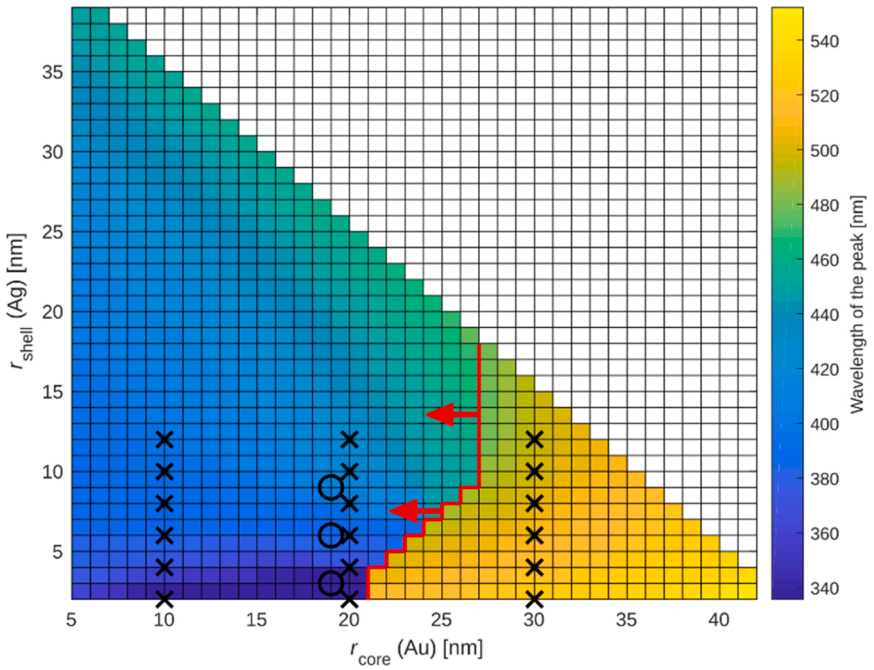

Fig. 2. The position of the most intense extinction peak as a function of core and shell radii for Au@Ag monomers. The 'O' marks indicate positions, where the effect of decreasing interparticle gap is investigated with high d/D_0 resolution (as presented in Fig. 10), 'X': indicate positions where the effect of shell thickness is investigated with lower d/D_0resolution (as presented in Fig. 11). (Reproduced from Ref. [3] under CC-BY license).

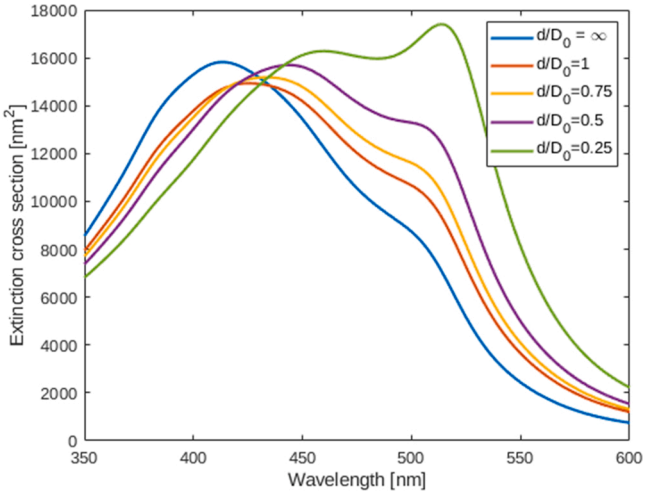

Fig. 3. Ag@Au, $r_c = 20\ nm$, $r_s = 4\ nm$: the extinction spectra characteristic of the thin shell range (with a peak transition).

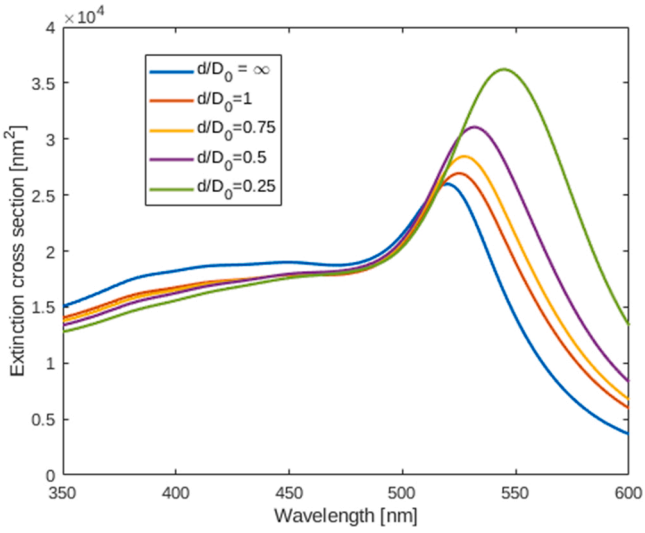

Fig. 4. Ag@Au, $r_c = 20\ nm$, $r_s = 10\ nm$: the extinction spectra characteristic of the thick shell range.

near-UV range of the spectrum. The peaks in the different groups also differ in terms of sensitivity.

3. Results

3.1. Monomers

Figs. 1 and 2 present the positions of the most intense extinction peaks as a function of core and shell radii for both the Ag@Au and Au@Ag type monomers. The position of the most intense peak can be assigned to either the Au (higher wavelengths) or the Ag (lower wavelengths) component, the red curve indicates the borderline between these distinct regions. (The bluish-colored ranges are dominated by Ag peaks, while the yellow color refers to the Au-type dominant peak.)

Almost all dominant peaks in the investigated size range can be attributed to the dipole mode. The origin of the peaks was identified by multipole decomposition of the extinction cross-sections of monomer core-shell particles. This calculation was performed with a program named 'scattnlay' which is based on the Mie-theory [35]. The few exceptions when not only dipole, but also a quadrupole peak appears are clearly indicated in the text.

To investigate the effect of decreasing interparticle gap, several (r_c, r_s) points were selected, as indicated with the markers and described in the figure captions. The red arrows indicate the direction where the borderline shifts with the decreasing interparticle gap. This effect will be elaborated on in detail in the following sections.

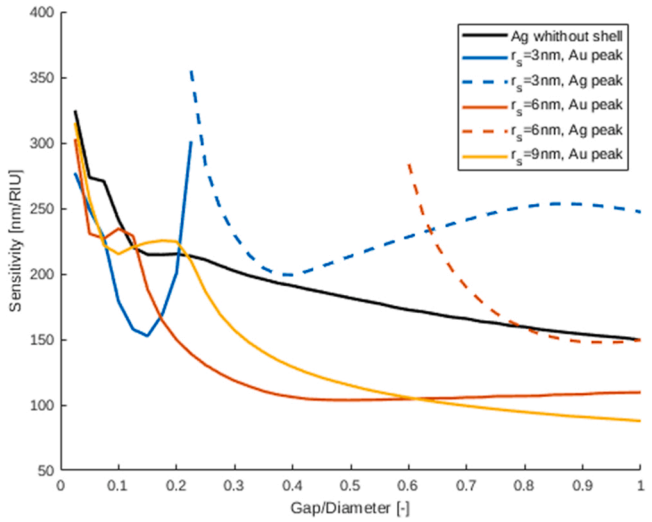

Fig. 5. Sensitivity of Ag@Au, $r_c = 22\,nm$, $r_s = (3,\ 6,\ 9)\,nm$ nanoparticles. (Simulated with high d/D_0 resolution).

3.2. Results on the dimer Ag@Au nanostructure system

3.2.1. Extinction spectrum of the dimer Ag@Au nanostructure system

Similar to the monomer particles in the previous section, both Ag and Au peaks can be observed for dimer particles too. Since the sensitivity of peaks corresponding to these components is significantly different, it is important to distinguish peaks that appear in different size ranges. In addition, the sensitivities differ from the one-particle case for multi-particle systems even if the same peak type appears. The presented data can help optimize interparticle gaps concerning the core/shell thicknesses to maximize the sensitivity of the dimer nanostructures.

All presented spectra were simulated in a dielectric environment

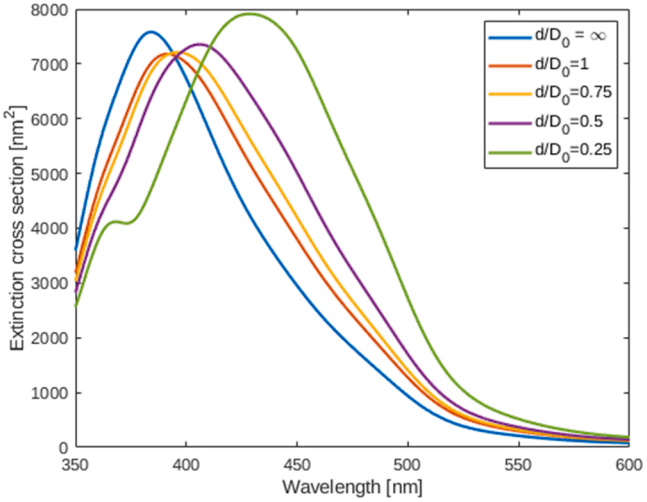

Fig. 7. Au@Ag, $r_c = 10\,nm$, $r_s = 6\,nm$: the extinction spectrum characteristic of the small core range.

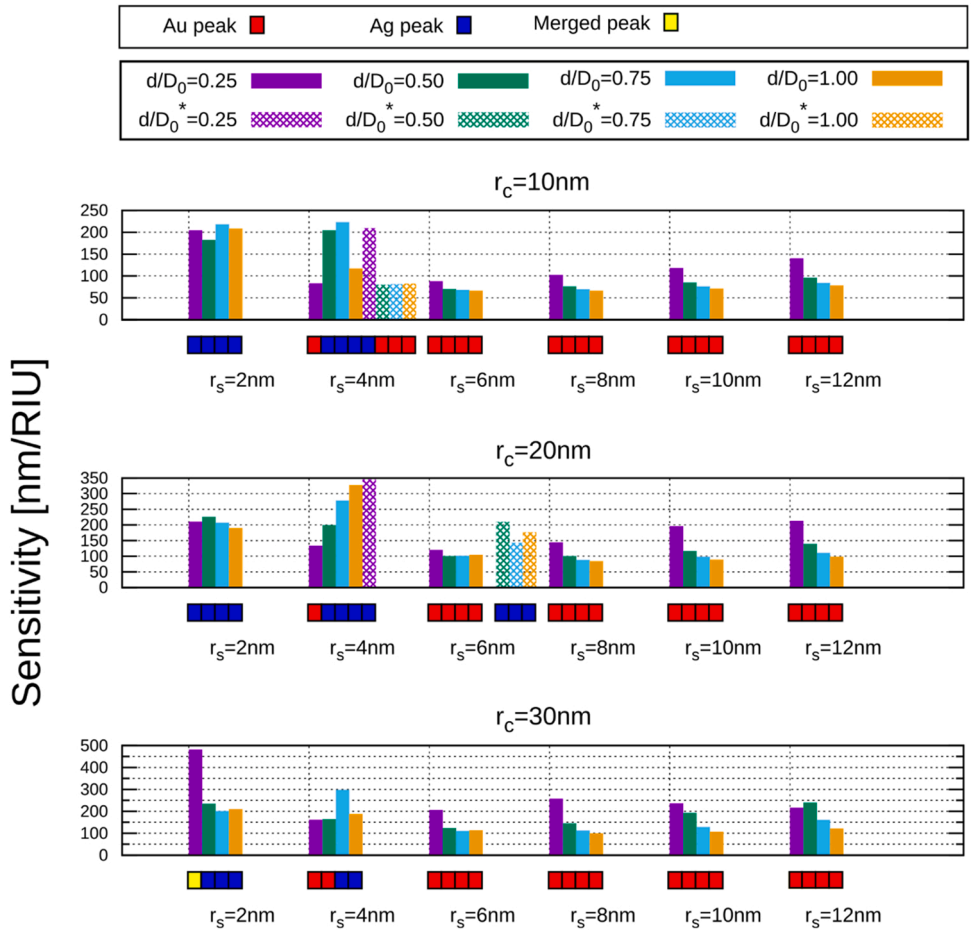

Fig. 6. Ag@Au sensitivities and peak types (the dominant peaks are marked with filled columns, the secondary peaks are marked with perforated columns and asterisks in text).

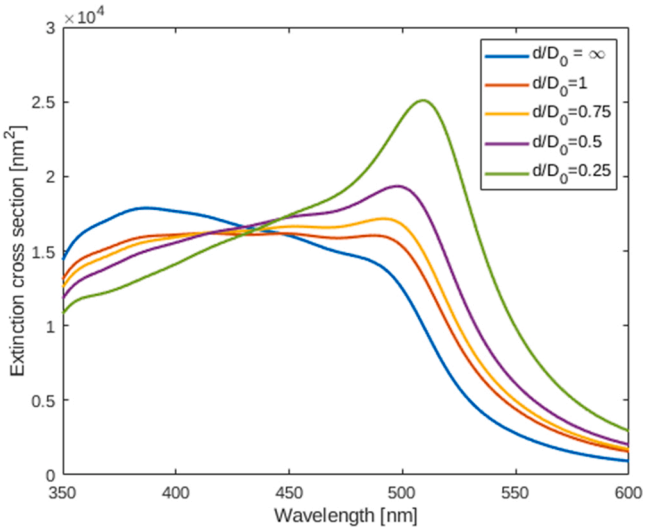

Fig. 8. Au@Ag, $r_c = 20\,nm$, $r_s = 6\,nm$: the transitional extinction spectrum.

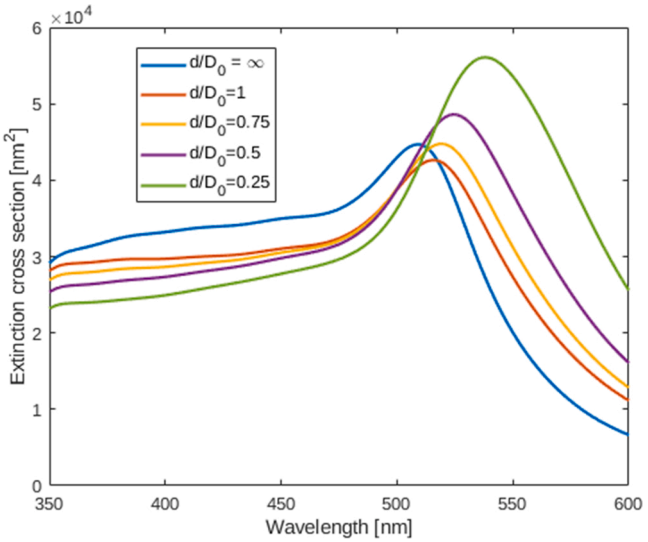

Fig. 9. Au@Ag, $r_c = 30\,nm$, $r_s = 6\,nm$: the extinction spectrum characteristic of the big core range.

with a refractive index of $n = 1.33$ curves in the figures show the monomer spectra multiplied by 2, corresponding to two infinitely distant nanoparticles.

The $r_c = 20\,nm$, $r_s = 4\,nm$ (see Fig. 3) system illustrates well the typical extinction spectra characteristic of thin shell thicknesses. By decreasing the interparticle gap, all appearing peaks shift towards longer wavelengths while the Au peak becomes increasingly dominant. So, at smaller distances, Au peaks dominate instead of Ag peaks.

If the silver core has a thick gold shell (see: Fig. 4), the transitions between the different peak types by changing the interparticle gap no longer occur. Decreasing the gap only increases the wavelength of the peak.

3.2.2. Sensitivity of the dimer Ag@Au nanostructure system

For monomer particles, sensitivity maxima appear along the boundary, which areas are of particular interest [14]. For a general description, r_c sites associated with high sensitivity for monomers were examined as a function of d/D_0 for multiple r_s values. The dependence of sensitivity on the interparticle gap has been described for a few typical cases, but all the phenomena described can be extended to a wider

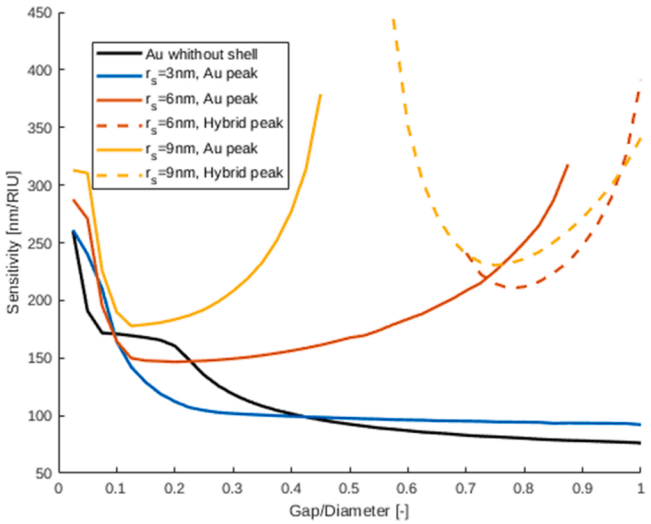

Fig. 10. Sensitivity of Au@Ag, $r_c = 19\,nm$, $r_s = (3,\ 6,\ 9)\,nm$ nanoparticles. (Simulated with high d/D_0 resolution).

range. To show the trends, the $r_c = 22\,nm$ case was selected with $r_s = (3, 6, 9)nm$ shells and the Ag dimer system without shells as a reference (see Fig. 5). If the shell is thick e.g. $r_s = 9\,nm$, a single Au peak appears, which is more sensitive for smaller gaps (see Fig. 6). In the other two cases, the increase in sensitivity to a given peak persists with decreasing distance, however, an Ag peak also appears. At a shell thickness of 3 nm, and d/D_0 value, where both the peaks are present simultaneously, the wavelengths of the two peaks are within 40 nm of each other. These peaks have roughly the same intensity and width. For more distant particles, the Ag peaks become increasingly significant, while the Au peaks become broad-shouldered. If multiple peaks appear, the usual d/D_0 dependence of the sensitivity changes, the sensitivity of both peaks increases.

By thickening the shell, the Au peak becomes dominant (see Fig. 6). This occurs at thinner shells in dimer systems than in monomer particles, i.e., a shift of the boundary separating domains towards smaller shells is observed (see Fig. 1). A change in the type of dominant peak as a result of increasing the thickness of the shell usually negatively affects the sensitivity, because usually, Au peaks are less sensitive than Ag peaks. If the gap is large, the nature of the change in sensitivity is similar to the not core-shell case until the peak dominance shift intervenes. The trend that the sensitivity of the closer nanoparticles is higher is not always fulfilled near the peak dominance transition. At small distances, often the lower sensitivity peak becomes dominant, e.g. ($r_c = 10\,nm$, $r_s = 4\,nm$), ($r_c = 20\,nm$, $r_s = 4\,nm$), ($r_c = 20\,nm$, $r_s = 6\,nm$). The small gap often leads to the complete disappearance of the more sensitive peak. Multiple peaks appear at the same time only for well-defined sizes and distances, specifically: ($r_c = 10\,nm$, $r_s = 4\,nm$), and ($r_c = 20\,nm$, $r_s = 6\,nm$). The sensitivity of the close particles is generally higher for all types of peaks. At: ($r_c = 30\,nm$, $r_s = 2\,nm$, $d/D_0 = 0.25$), the two peaks merge, causing unusually high sensitivity.

3.3. Results on the dimer Au@Ag nanostructure system

3.3.1. Extinction spectrum of the dimer Au@Ag nanostructure system

In terms of peak type, for Au@Ag composition, the size of the core is the most important parameter. The shell $r_s = 6\,nm$ was selected for a generalized spectrum description, however, it should be noted that in the case of Au@Ag it is a worse approximation to designate a range-specific spectrum than in the previous chapter. For a more complete description, the results are presented for three different core sizes. The most characteristic feature of the Ag@Au case is the extreme broadening of the silver peak, which is the most significant close to the $r_c = 20\,nm$

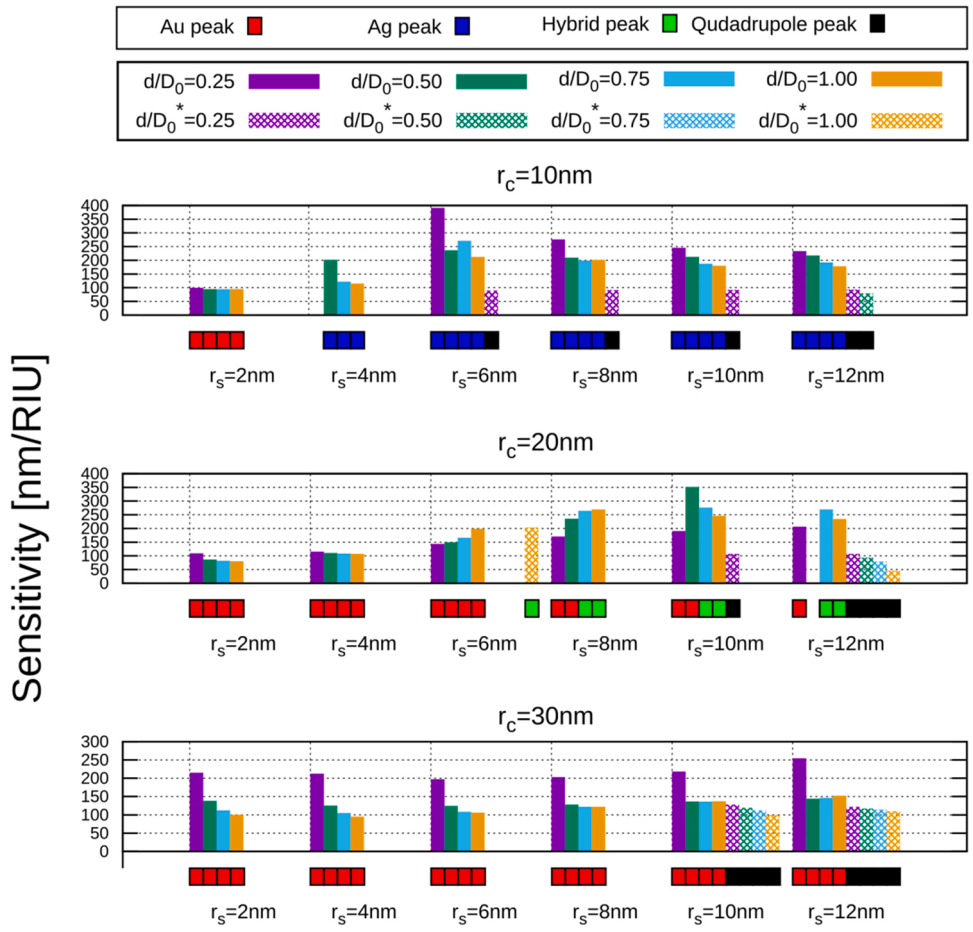

Fig. 11. Au@Ag sensitivities and peak types. (The dominant peaks are marked with filled columns, the secondary peaks are marked with perforated columns and asterisks in text).

core size.

If the core is small e.g. $r_c = 10\,nm$, Ag peaks are characteristic (see Fig. 7). At $d/D_0 = 0.25$ a small quadrupole peak in the near-UV appears uniquely among the extinction figures.

Transitional extinction spectrum can be observed for particles with medium-sized core e.g. $r_c = 20\,nm$ (see Fig. 8). The extinction curves flatten out, smaller hybrid peaks that do not belong to the two main categories appear. These phenomena occur especially at greater distances, where the interparticle gap is comparable to the diameter of the nanoparticles. The dominance transition does not directly occur between the Ag and Au peaks, but the transition boundary becomes slightly blurred: as the spectra flatten out, hybrid peaks sometimes become dominant. However, in the long run, there is a tendency for the Ag and hybrid peaks to disappear eventually and the Au peak to intensify.

For large cores e.g. $r_c = 30\,nm$ only the gold peak remains (see Fig. 9). As the distance decreases, the peaks are found at increasingly long wavelengths.

3.3.2. *Sensitivity of the dimer Au@Ag nanostructure system*

To present trends in the sensitivity, $r_c = 19\,nm$ was selected with $r_s = (3, 6, 9)nm$ shells and the Au nanoparticle dimers without shells as a reference (Fig. 10). Applying a 3 nm shell to the core does not cause a significant change in sensitivity compared to the purely gold particle. Transient spectra, as shown in Fig. 8, was observed for $r_s = (6, 9)nm$. The transition in peak dominance greatly increases the sensitivity, but it also means the flattening of the extinction curve, which is not advantageous in practical use. This phenomenon is so significant that the sensitivity cannot be evaluated in all cases if the shell thickness is $r_s = 9\,nm$.

The results collected over a larger size range are consistent with those described so far (see Fig. 11). Between $r_c = 20nm$ and $30nm$, a jump at long distances can be seen in wavelengths at $r_s = 4nm$ and thicker shells, suggesting a change in peak dominance as a function of r_c. The boundary line separating the range of different peaks shifted slightly towards smaller cores compared to the monomer case. Due to the variety of peaks that appear, the description of Ag@Au particles is more complicated than what was seen for Ag@Au. At higher wavelength peaks, the sensitivity is usually lower, so in many cases increasing the core is particularly disadvantageous in terms of sensitivity. The thickening of the shell leads to a strengthening of the silver character, thus reducing the wavelength of the peaks. In terms of sensitivity, a thicker shell is better, however, a significant widening of the peaks can also be observed. For small d/D_0, the peaks are found at high wavelengths, as in the case of a non-core-shell dimer. The distance dependence of the sensitivity is anomalous in a few cases, especially when $r_c = 20nm$. At these locations, the emerging hybrid peaks cause the anomaly. The flattening of the spectrum is always characteristic in this case. This effect made the main peak invaluable when ($r_c = 20nm, r_s = 12nm$). If the Ag shell is thick, peaks also appear in the near-UV range, however, these small quadrupole peaks are not prominent in terms of sensitivity either.

4. Conclusions

Gold-silver, silver-gold core-shell, nanoparticle dimers were studied for their extinction cross-section spectrum and bulk refractive index sensitivity. The results were presented for both Ag@Au and Au@Ag cases. Based on the results obtained previously for monomers [14] nanoparticles were selected that represent the different size domains

well. In the plane of the core radius and shell thickness parameters, the particles can be assigned to one of two regions based on their most intense extinction peak. The regions were classified according to the origin of the dominant peak: Ag peak or Au peak and have different characteristics. It was found that the boundary line between the two regions for Ag@Au dimers shifts towards the thinner shells by reducing the distance between the particles, while for Au@Ag it shifts towards the smaller cores. Thus, in both Ag@Au and Au@Ag cases, nanoparticle dimers have Au-related peaks over a larger size range than monomers.

At the boundaries of the regions, the sensitivity typically increases, however, the widening of the peaks can also be observed. Distance-dependent phenomena: redshift, increased sensitivity is observed for non-core-shell particles persist approximately at the locations characterized by a single peak. However, when multiple peaks appear, the situation is different.

For the inner regions of the domains, it is generally true that in the case of Ag@Au, nanoparticles with a large core and thin shell composition are more sensitive. The sensitivity can be increased by reducing the distance, as long as it does not cause a change in the type of the most intense peak. A gold shell can also be used to chemically protect the silver core or achieve biocompatibility; however, if the shell is too thick or the particles are too close, the more sensitive silver peak may disappear.

In the case of Au@Ag, apart from the transition region, the smaller core and thicker shell arrangements are more sensitive. Reducing the gap between the particles is not always recommended in this case, because an amplified Au peak is less sensitive than the disappearing Ag peak.

Conclusively, it was demonstrated that by proper core-shell thickness design and careful interparticle gap engineering, the bulk refractive index sensitivity of Au@Ag and Ag@Au core-shell dimer systems could be increased significantly. Nanoparticle gap engineering with sub-nanometer resolution can be performed experimentally in liquid phase by using DNA linkers [39]. The resulting RIS of 200–400 nm/RIU is relevant for most chemical and biosensing applications, although it is still lower compared to classical, thin-film-based SPR devices (in the 3000–4000 nm/RIU range) [40]. As established previously, the molecular sensitivity of LSPR sensors with similar RIS can match or even surpass the molecular sensitivity of SPR devices [40].

Declaration of Competing Interest

The authors declare that they have no known competing financial interests or personal relationships that could have appeared to influence the work reported in this paper.

Acknowledgments

We acknowledge KIFÜ for awarding us access to resource-based in Hungary.

This work was supported by the GINOP-2.3.2–15-2016-00041 Project, which is co-financed by the European Union and the European Regional Development Fund. Istvan Csarnovics is grateful for the support of the János Bolyai Research Scholarship of the Hungarian Academy of Sciences (BO/348/20) and the support through the New National Excellence Program of the Ministry of Human Capacities (ÚNKP-21-5-DE-164).

This research was supported by the EU-funded Hungarian Grant EFOP-3.6.2-16-2017-00005.

The research reported in this paper and carried out at the Budapest University of Technology and Economics was funded by the National Research, Development, and Innovation Fund of Hungary under Grant TKP2021-EGA-02. This work was partially supported by Nanoplasmonic Laser Fusion Research Laboratory project financed by the National Research and Innovation Office (NKFIH-468-3/2021) and by the Eötvös Loránd Research Network (ELKH), Hungary. Attila Bonyár and Géza Szántó are grateful to the Deutscher Akademischer Austauschdienst (DAAD, Germany) and Tempus Public Foundation (TKA, Hungary) for supporting the “Development of plasmonic hybrid optical biosensors” (TKA-160590) bilateral project.

Appendix A. MFP correction

The results reported in this article are based on the tables of complex refractive indices of metals provided by Johnson & Christy [29]. It was pointed out in the paper that the results obtained for layer thicknesses slightly above 30 nm, already describe the properties of bulk metals. However, for thinner layers, the optical properties may change compared to the bulk case [29].

In the present article, properties of particles with shells in the range of a few nm and also with small core sizes have been studied. Therefore, the question of applying electron mean free path corrections rightfully arises. The problem is mainly caused by the fact that the studied dimensions are significantly below the mean free path length of the electrons for both gold and silver in many cases.

Correction for free path effects can be performed for spherical core-shell particles based on the work of Rasskazov et al. [33]. The subject of the cited article is a MATLAB code for multilayer spheres, and the source code is made available by the authors [36]. We used part of this code to implement the free path correction with the modification of the MNPBEM toolbox [27]. Among the Drude fit parameters, the values of Blaber et. al was selected for testing [37]. The correction was applied to both the core and the shell in each case.

Since the simulations take a long time to run, the complete review of all the results presented in the article is impossible. However, a few typical cases have been corrected, and these examples show that the effect of the correction is almost negligible. The effect of the correction on both the extinction cross-section spectrum and the sensitivity is presented here. Sample particle systems that were presented in the article were selected for demonstration here for the sake of direct comparability.

A comparison of corrected and uncorrected results is presented below:

A.1. Ag@Au

A.1.1. $r_c = 20$ nm, $r_s = 4$ nm

Considering the effect of the electron mean free path, the height of the peaks in the extinction spectra is modified a bit, but the shape of the spectra does not change significantly. There is no shift in the position of the peaks, but the height is slightly lower as a result of the correction (Fig. A.1).

A.1.2. $r_c = 20$ nm, $r_s = 10$ nm

As the thickness of the gold shell increases, the correction matches the original simulated extinction spectrum even better (Fig. A.2).

A.1.3. Sensitivity

The effect of the correction on sensitivity is so tiny that it is difficult to see in the figures, only deviations of up to a few nm/RIU occur as a result of the corrections (Fig. A.3).

A.2. Au@Ag

A.2.1. $r_c = 10$ nm, $r_s = 6$ nm

The relative heights of the peaks, in this case, were modified the most of all the particle systems examined. This may be because here not only the thinness of the silver shell plays a role in modifying the results, but also the small radius of the gold core. Again, only the height of the peaks is changed, the position is not (Fig. A.4).

A.2.2. $r_c = 20$ nm, $r_s = 6$ nm

Due to the increased core, in this case, the difference between the two results decreases is and mostly caused by the 6 nm shell (Fig. A.5).

A.2.3. $r_c = 30$ nm, $r_s = 6$ nm

The difference between the corrected and uncorrected extinction spectra for such particle sizes is negligible (Fig. A.6).

A.2.4. Sensitivity

In terms of sensitivity, the Au@Ag nanoparticles also show no significant difference between the results. The only detectable change is present for the ($r_c = 10$ nm and $d/D_0 = 0.25$) system, where there is a small peak at 370 nm without correction, which is not found when a correction is applied (the curve has no local maximum there, only a small plateau is present.) (Fig. A.7).

A.3. Conclusion

Based on the presented systems, it can be presumed that neglecting the mean free path correction does not significantly affect the results of the simulations, especially considering the sensitivity of the coupled core-shell dimers.

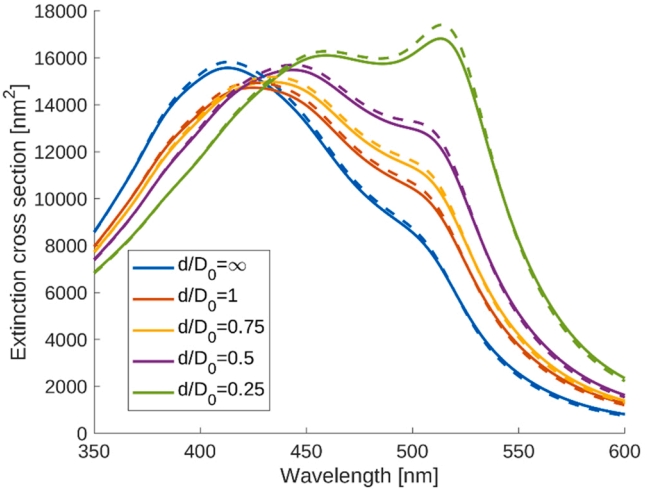

Fig. A.1. Ag@Au, $r_c = 20$ nm, $r_s = 4$ nm (solid line: corrected, dashed line: without correction).

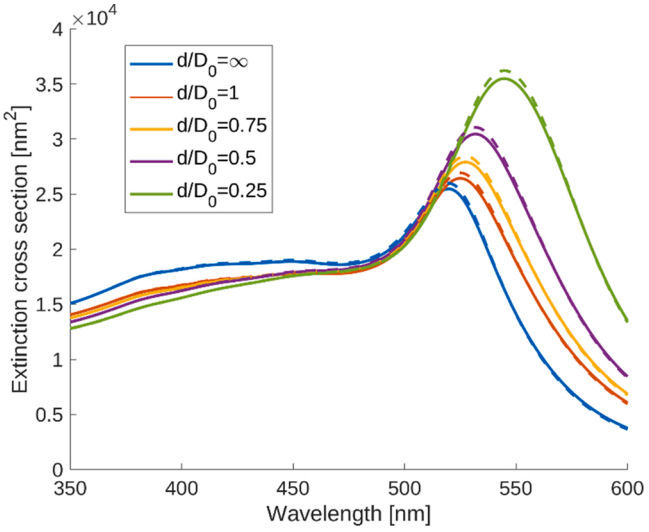

Fig. A.2. Ag@Au, $r_c = 20$ nm, $r_s = 10$ nm (solid line: corrected, dashed line: without correction).

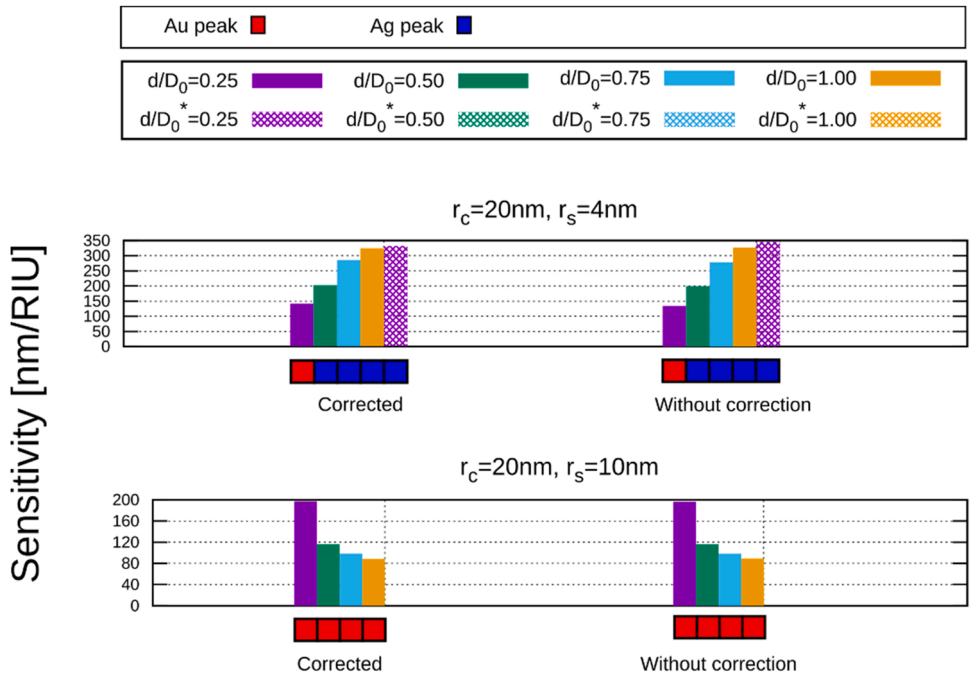

Fig. A.3. Ag@Au sensitivities and peak types. (The dominant peaks are marked with filled columns, the secondary peaks are marked with perforated columns and asterisks in text).

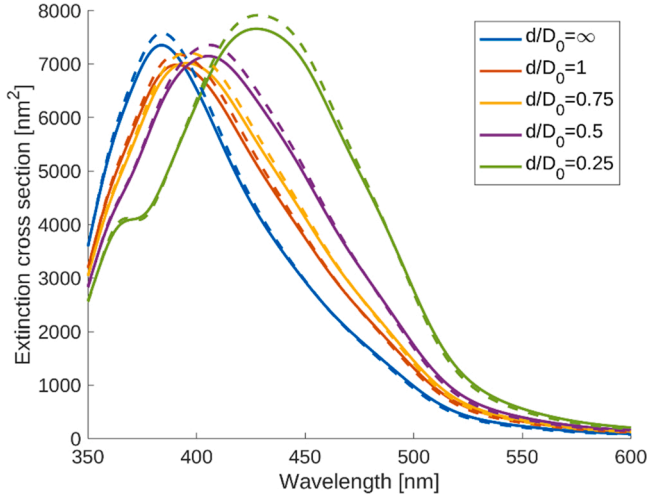

Fig. A.4. Au@Ag, r_c = 10 nm, r_s = 6 nm (solid line: corrected, dashed line: without correction).

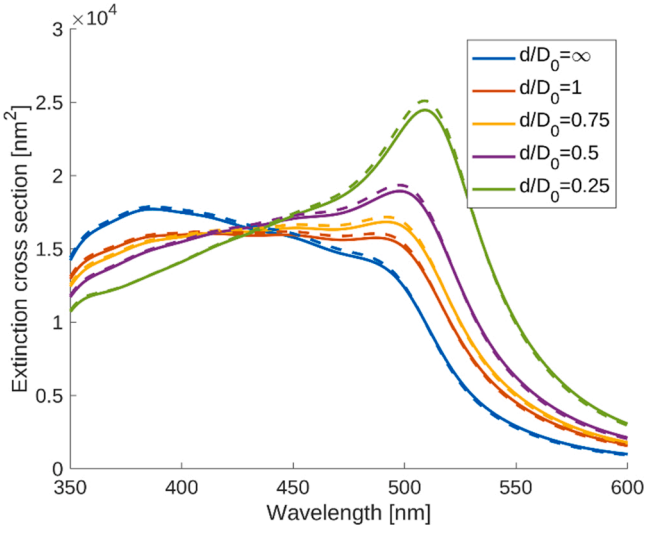

Fig. A.5. Au@Ag, r_c = 20 nm, r_s = 6 nm (solid line: corrected, dashed line: without correction).

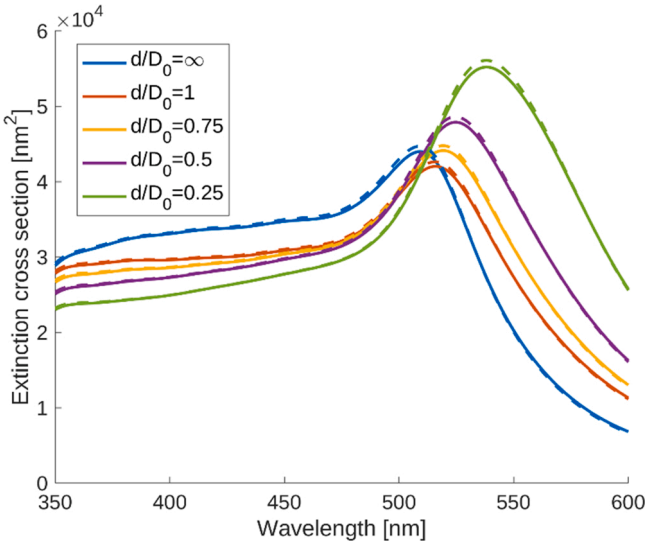

Fig. A.6. Au@Ag, $r_c = 30$ nm, $r_s = 6$ nm (solid line: corrected, dashed line: without correction).

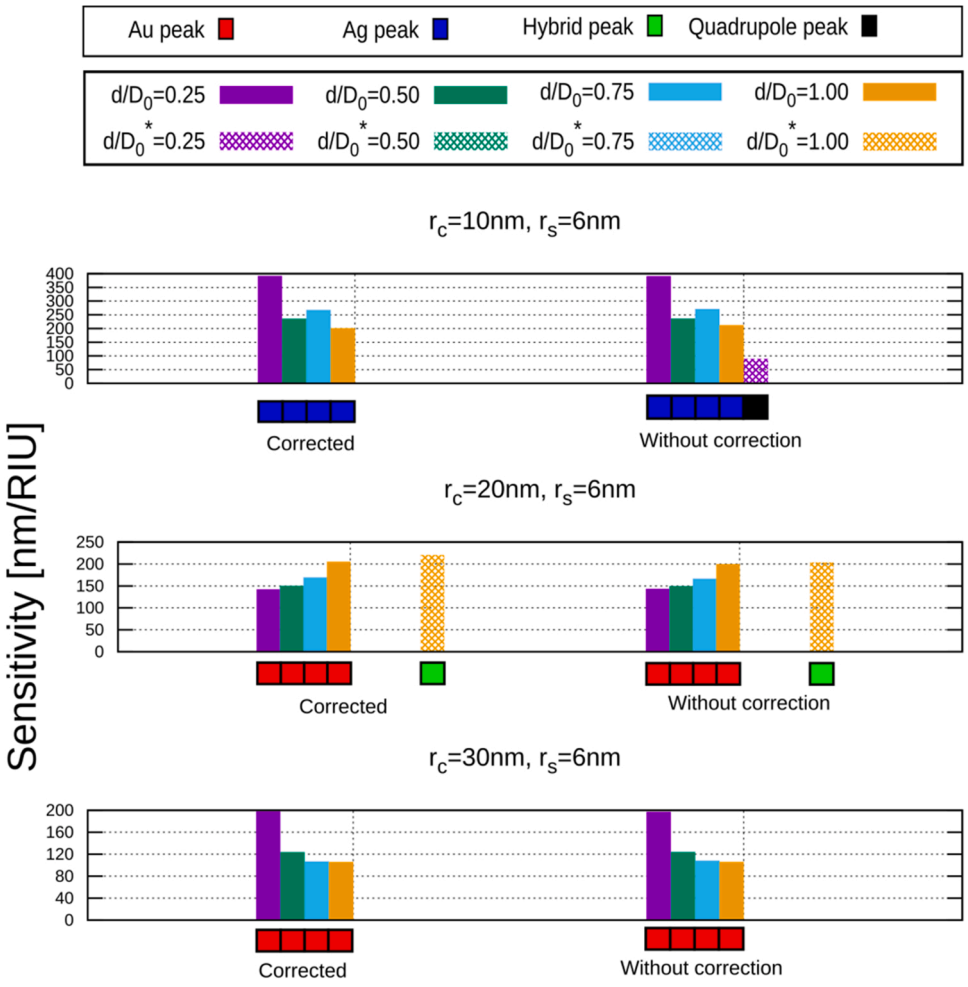

Fig. A.7. Au@Ag sensitivities and peak types. (The dominant peaks are marked with filled columns, the secondary peaks are marked with perforated columns and asterisks in text).

Appendix B. Quasistatic approximation

Special cases of the studied core-shell systems can be studied without simulation. Such approximation methods can be valuable tools, but only if their scope can be precisely defined. The quasistatic approximation, which is suitable for studying small monomer core-shell particles, can only be applied if the particle is significantly smaller than the wavelength of the excitation light. According to our simulations, the method gives an accurate result for monomer core-shell particles up to a total radius of (10-15) nm.

The same result as the simulation can be obtained by the Mie-theory, so the following can also be considered as a Mie - quasistatic comparison [35].

The basis of the approximation is that the scattering can be described in terms of Rayleigh scattering so, on a particle a single dipole is induced.

B.1. Calculations

The presented calculations are based on the classic book of Bohren and Huffman [38]. As a first step, dipolar polarizability of a single homogeneous sphere with *r* radius was calculated.

$$\alpha_s = 4\pi r^3 \frac{\epsilon - \epsilon_m}{\epsilon + 2\epsilon_m}$$

Where ϵ_k is the permittivity of (no index: nanoparticle, m: medium). The formula of polarizability can be extended to core-shell particles as follows:

$$\alpha_{cs} = 4\pi(r_c + r_s)^3 \frac{(\epsilon_s - \epsilon_m)(\epsilon_c + 2\epsilon_s) + f(\epsilon_c - \epsilon_s)(\epsilon_m + 2\epsilon_s)}{(\epsilon_s + \epsilon_m)(\epsilon_c + 2\epsilon_s) + f(2\epsilon_s - 2\epsilon_m)(\epsilon_c - \epsilon_s)}$$

where the f parameter is:

$$f = \frac{r_c^3}{(r_c + r_s)^3} = \frac{V_c}{V_{cs}}$$

The (a: absorption, s: scattering, e: extinction) cross-sections can be calculated from the polarizability:

$$\sigma_a = k\Im(\alpha)$$

$$\sigma_s = \frac{k^4}{6\pi}|\alpha|^2$$

$$\sigma_e = \sigma_a + \sigma_s$$

Where *k* is the wavenumber $k = 2\pi/\lambda_m = n \cdot 2\pi/\lambda$ (λ_m is the wavelength in the medium, λ is the wavenumber in vacuum).

For small particles where the model is valid, σ_s is negligible, so $\sigma_e \approx \sigma_a$ so, the extinction spectrum comes from the imaginary part of the polarization.

B.2. Quasistatic results

B.2.1. Simple sphere

Simple spherical particles were first studied to determine the scope of the method. Even for these particles, the quasistatic approximation gives good results only for very small radii. In other cases, it does not give a correct result for the shifting and widening of the peak, this is especially true for silver particles (Figs. B1 and B2).

For $r > 30$ nm silver particles, in addition to the dipole attributed peak, a quadrupole attributed peak also appears at short wavelengths. This peak is, of course, not observable by the quasistatic method.

B.2.2. Core-shell particle

In contrast, in the case of homogeneous spheres, several peaks may appear on the extinction spectrum of core-shell particles, even for quasistatic approximation. It can be observed, as expected, that the quasistatic approximation gives good results for small particles. The difference depends not only on the particle size between the approximation and the simulation: when the silver core or shell is small, i.e., the particle is mainly gold, the approximation gives a more reliable result (Figs. B3 and B4).

This analytical method presented in the appendix, despite its limitations, may be useful in the study of light scattering and absorption phenomena.

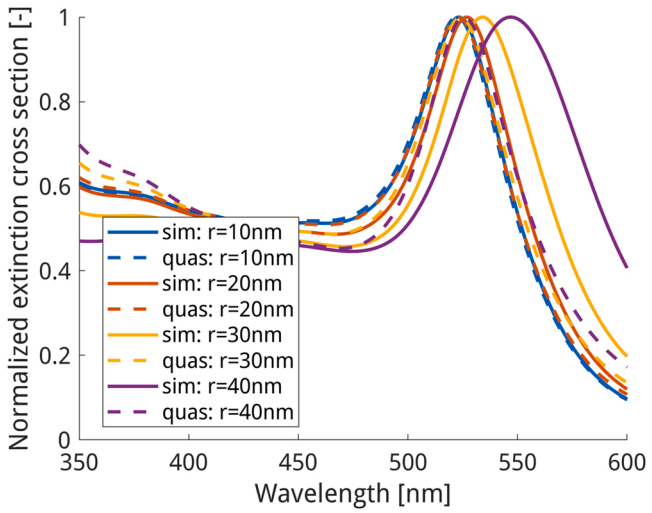

Fig. B1. Normalized extinction cross-sections of Au particles by quasistatic approximation and simulation.

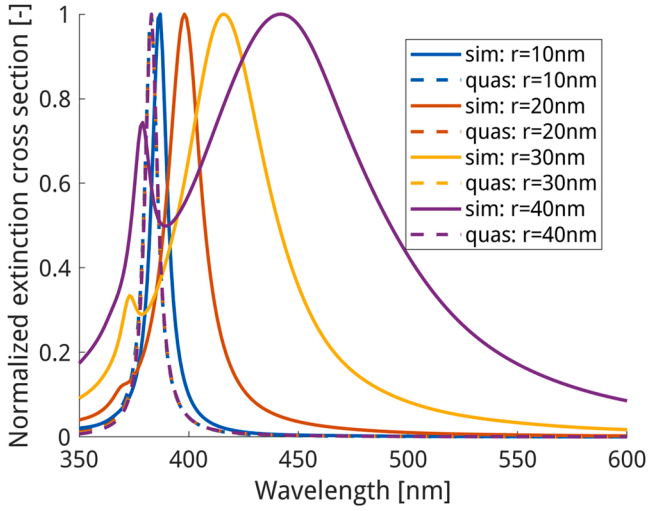

Fig. B2. Normalized extinction cross-sections of Ag particles by quasistatic approximation and simulation.

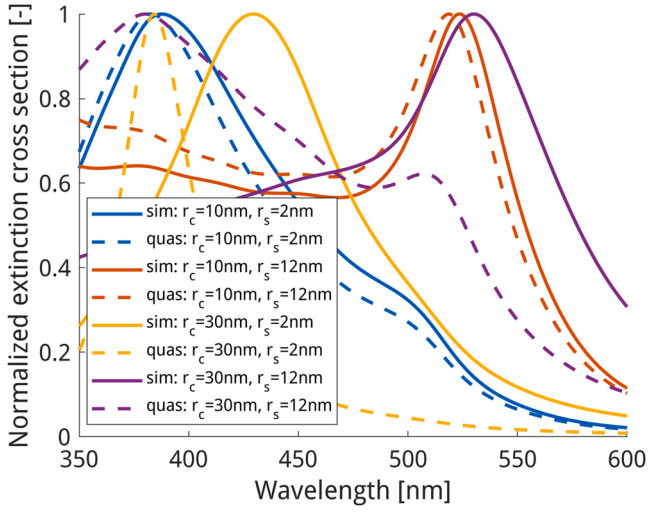

Fig. B3. Normalized extinction cross-sections of core-shell particles by quasistatic approximation and simulation Ag@Au.

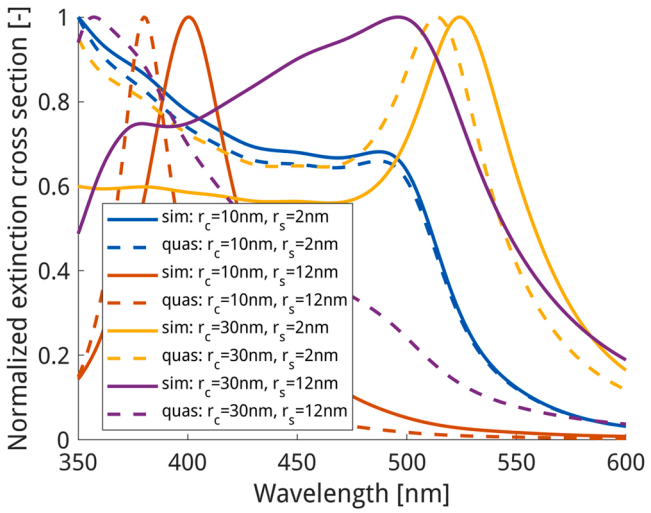

Fig. B4. Normalized extinction cross-sections of core-shell particles by quasistatic approximation and simulation Au@Ag.

References

[1] S. Szunerits, R. Boukherroub, Sensing using localised surface plasmon resonance sensors, Chem. Commun. 48 (72) (2012) 8999, https://doi.org/10.1039/c2cc33266c.

[2] M.M. Miller, A.A. Lazarides, Sensitivity of metal nanoparticle surface plasmon resonance to the dielectric environment, J. Phys. Chem. B 109 (46) (2005) 21556–21565, https://doi.org/10.1021/jp054227y.

[3] M. Duval Malinsky, K.L. Kelly, G.C. Schatz, R.P. Van Duyne, Nanosphere lithography: effect of substrate on the localized surface plasmon resonance spectrum of silver nanoparticles, J. Phys. Chem. B, 105(12), 2001, pp. 2343–2350. ⟨10.1021/jp002906x⟩.

[4] V. Amendola, R. Pilot, M. Frasconi, O.M. Maragò, M.A. Iatì, Surface plasmon resonance in gold nanoparticles: a review, J. Phys.: Condens. Matter 29 (20) (2017), 203002, https://doi.org/10.1088/1361-648X/aa60f3.

[5] B. Liedberg, C. Nylander, I. Lundström, Biosensing with surface plasmon resonance — how it all started, Biosens. Bioelectron., 10(8), 1995, pp. i–ix. ⟨10.1016/0956-5663(95)96965-2⟩.

[6] I. Lundström, From a laboratory exercise for students to a pioneering biosensing technology, Plasmonics 9 (4) (2014) 741–751, https://doi.org/10.1007/s11468-013-9654-3.

[7] A. Bonyár, Label-free nucleic acid biosensing using nanomaterial-based localized surface plasmon resonance imaging: a review," ACS Appl. Nano Mater., 3(9), 2020, pp. 8506–8521. ⟨10.1021/acsanm.0c01457⟩.

[8] J. Prinz, C. Heck, L. Ellerik, V. Merk, I. Bald, DNA origami based Au–Ag-core–shell nanoparticle dimers with single-molecule SERS sensitivity, Nanoscale, 8(10), 2016, pp. 5612–5620. ⟨10.1039/C5NR08674D⟩.

[9] A. Sakthisabarimoorthi, S.A. Martin Britto Dhas, M. Jose, Preparation of composite Ag@Au core–shell nanoparticles and their linear and nonlinear optical properties, J. Mater. Sci.: Mater. Electron. 30 (2) (2019) 1677–1685, https://doi.org/10.1007/s10854-018-0439-5.

[10] A.-M. Hada, et al., Fabrication of gold–silver core–shell nanoparticles for performing as ultrabright SERS-nanotags inside human ovarian cancer cells, Nanotechnology 30 (31) (2019), 315701, https://doi.org/10.1088/1361-6528/ab1857.

[11] A.K. Samal, L. Polavarapu, S. Rodal-Cedeira, L.M. Liz-Marzán, J. Pérez-Juste, I. Pastoriza-Santos, Size tunable Au@Ag core–shell nanoparticles: synthesis and surface-enhanced Raman scattering properties, Langmuir 29 (48) (2013) 15076–15082, https://doi.org/10.1021/la403707j.

[12] H. Lee, J.-H. Lee, S.M. Jin, Y.D. Suh, J.-M. Nam, Single-molecule and single-particle-based correlation studies between localized surface plasmons of dimeric nanostructures with ~1 nm gap and surface-enhanced raman scattering, Nano Lett. 13 (12) (2013) 6113–6121, https://doi.org/10.1021/nl4034297.

[13] E. Seo, S.-J. Ko, S.H. Min, J.Y. Kim, B.-S. Kim, Plasmonic transition via interparticle coupling of Au@Ag core–shell nanostructures sheathed in double hydrophilic block copolymer for high-performance polymer solar cell, Chem. Mater., 27(13), 2015, pp. 4789–4798. ⟨10.1021/acs.chemmater.5b01591⟩.

[14] G. Szántó, I. Csarnovics, A. Bonyár, Numerical investigation of the refractive index sensitivity of Au/Ag core-shell nanostructures (for sensing applications), Sens. Bio-Sens. Res 32 (2021) 100414, https://doi.org/10.1016/j.sbsr.2021.100414.

[15] N.J. Halas, S. Lal, W.-S. Chang, S. Link, P. Nordlander, Plasmons in strongly coupled metallic nanostructures, Chem. Rev., 111(6), 2011, pp. 3913–3961. ⟨10.1021/cr200061k⟩.

[16] K.-H. Su, Q.-H. Wei, X. Zhang, J.J. Mock, D.R. Smith, S. Schultz, Interparticle coupling effects on plasmon resonances of nanogold particles, Nano Lett. 3 (8) (2003) 1087–1090, https://doi.org/10.1021/nl034197f.

[17] P.K. Jain, W. Huang, M.A. El-Sayed, On the universal scaling behavior of the distance decay of plasmon coupling in metal nanoparticle pairs: a plasmon ruler equation, Nano Lett., 7(7), 2007, pp. 2080–2088. ⟨10.1021/nl071008a⟩.
[18] P.K. Jain, M.A. El-Sayed, Universal scaling of plasmon coupling in metal nanostructures: extension from particle pairs to nanoshells, Nano Lett., 7(9), 2007, pp. 2854–2858. ⟨10.1021/nl071496m⟩.
[19] W. Park, Optical interactions in plasmonic nanostructures, Nano Converg., 1(1), 2014. ⟨10.1186/s40580-014-0002-x⟩.
[20] P.K. Jain, M.A. El-Sayed, Plasmonic coupling in noble metal nanostructures, Chem. Phys. Lett., 487(4–6), 2010, pp. 153–164. ⟨10.1016/j.cplett.2010.01.062⟩.
[21] A. Bonyár, Simulation of the refractive index sensitivity of coupled plasmonic nanostructures, Procedia Eng., 168, 2016, pp. 962–965. ⟨10.1016/j.proeng.2016.11.316⟩.
[22] O. Peña-Rodríguez, U. Pal, Enhanced plasmonic behavior of bimetallic (Ag-Au) multilayered spheres, Nanoscale Res. Lett. 6 (1) (2011) 279, https://doi.org/10.1186/1556-276X-6-279.
[23] P. Nordlander, C. Oubre, E. Prodan, K. Li, M.I. Stockman, Plasmon hybridization in nanoparticle dimers, Nano Lett. 4 (5) (2004) 899–903, https://doi.org/10.1021/nl049681c.
[24] M. Pascale, G. Miano, R. Tricarico, C. Forestiere, Full-wave electromagnetic modes and hybridization in nanoparticle dimers, Sci. Rep. 9 (1) (2019) 14524, https://doi.org/10.1038/s41598-019-50498-1.
[25] D. Chahinez, T. Reji, R. Andreas, Modeling of the surface plasmon resonance tunability of silver/gold core–shell nanostructures, RSC Adv., 8(35), 2018, pp. 19616–19626. ⟨10.1039/C8RA03261K⟩.
[26] F.J. García de Abajo, A. Howie, Retarded field calculation of electron energy loss in inhomogeneous dielectrics, Phys. Rev. B, 65(11), 2002, p. 115418. ⟨10.1103/PhysRevB.65.115418⟩.
[27] U. Hohenester, A. Trügler, MNPBEM – a Matlab toolbox for the simulation of plasmonic nanoparticles, Comput. Phys. Commun., 183(2), 2012, pp. 370–381. ⟨10.1016/j.cpc.2011.09.009⟩.
[28] Y. Cheng, M. Wang, G. Borghs, H. Chen, Gold nanoparticle dimers for plasmon sensing, Langmuir, 27(12), 2011, pp. 7884–7891. ⟨10.1021/la200840m⟩.
[29] P.B. Johnson, R.W. Christy, Optical constants of the noble metals, Phys. Rev. B, 6 (12), 1972, pp. 4370–4379. ⟨10.1103/PhysRevB.6.4370⟩.
[30] Y. Yang, et al., A general theoretical and experimental framework for nanoscale electromagnetism, Nature, 576(7786), 2019, pp. 248–252. ⟨10.1038/s41586-019-1803-1⟩.
[31] N.A. Mortensen, Mesoscopic electrodynamics at metal surfaces: — from quantum-corrected hydrodynamics to microscopic surface-response formalism, Nanophotonics, 10(10), 2021, pp. 2563–2616. ⟨10.1515/nanoph-2021-0156⟩.
[32] A. Moroz, Electron mean free path in a spherical shell geometry, J. Phys. Chem. C, 112(29), 2008, pp. 10641–10652. ⟨10.1021/jp8010074⟩.
[33] I.L. Rasskazov, P.S. Carney, A. Moroz, STRATIFY: a comprehensive and versatile MATLAB code for a multilayered sphere, OSA Contin., 3(8), 2020, p. 2290. ⟨10.1364/OSAC.399979⟩.
[34] W. Zhu, et al., Quantum mechanical effects in plasmonic structures with subnanometre gaps, Nat. Commun., 7, 2016, p. 11495. ⟨10.1038/ncomms11495⟩.
[35] K. Ladutenko, U. Pal, A. Rivera, O. Peña-Rodríguez, Mie calculation of electromagnetic near-field for a multilayered sphere, Comput. Phys. Commun., 214, 2017, pp. 225–230. ⟨10.1016/j.cpc.2017.01.017⟩.
[36] Ilia Rasskazov, STRATIFY, GitLab. [Online]. Available: ⟨https://gitlab.com/iliarasskazov/stratify⟩. (Accessed 23 September 2021).
[37] M.G. Blaber, M.D. Arnold, M.J. Ford, Search for the ideal plasmonic nanoshell: the effects of surface scattering and alternatives to gold and silver, J. Phys. Chem. C, 113(8), 2009, pp. 3041–3045. ⟨10.1021/jp810808h⟩.
[38] C.F. Bohren, D.R. Huffman, Absorption and Scattering of Light By Small Particles, Wiley, 1998, pp. 136–149.
[39] S. Lee, K. Sim, S.Y. Moon, J. Choi, Y. Jeon, J. Nam, S. Park, Controlled assembly of plasmonic nanoparticles: from static to dynamic nanostructures, Adv. Mater. (2021), 2007668, https://doi.org/10.1002/adma.202007668.
[40] M. Svedendahl, S. Chen, A. Dmitriev, M. Käll, Refractometric sensing using propagating versus localized surface plasmons: a direct comparison, Nano Lett. 9 (2009) 4428–4433.